TOXICOLOGICAL SCIENCES, 164(1), 2018, 264–277

doi: 10.1093/toxsci/kfy081
Advance Access Publication Date: April 4, 2018
Research Article

Developmental Exposure to Aluminum Chloride Irreversibly Affects Postnatal Hippocampal Neurogenesis Involving Multiple Functions in Mice

Mari Inohana,* Ayumi Eguchi,* Misato Nakamura,* Rei Nagahara,* Nobuhiko Onda,* Kota Nakajima,*,† Yukie Saegusa,‡ Toshinori Yoshida,* and Makoto Shibutani*,§,1

*Laboratory of Veterinary Pathology, Division of Animal Life Science, Institute of Agriculture, Tokyo University of Agriculture and Technology, Fuchu-shi, Tokyo 183-8509, Japan; †Pathogenetic Veterinary Science, United Graduate School of Veterinary Sciences, Gifu University, Gifu-shi, Gifu 501-1193, Japan; ‡Environment Health and Safety Division, Environment Directorate, OECD, 75775 Paris Cedex 16, France; and §Institute of Global Innovation Research, Tokyo University of Agriculture and Technology, Fuchu-shi, Tokyo 183-8509, Japan

[1]To whom correspondence should be addressed at Laboratory of Veterinary Pathology, Division of Animal Life Science, Institute of Agriculture, Tokyo University of Agriculture and Technology, 3-5-8 Saiwai-cho, Fuchu-shi, Tokyo 183-8509, Japan. Fax: +81-42-367-5771. E-mail: mshibuta@cc.tuat.ac.jp.

ABSTRACT

Aluminum (Al) is neurotoxic to adults and also to infants. In this study, we investigated the developmental exposure effect of $AlCl_3$ on postnatal hippocampal neurogenesis. Pregnant mice were administered 0-, 900-, or 1800-ppm $AlCl_3$ via drinking water from gestational day 6 to postnatal day (PND) 21, with their offspring examined on PND 21 and PND 77. On PND 21, GFAP-immunoreactive $^{(+)}$ neural stem cells (NSCs) and $p21^{Cip1/Waf1+}$ cells were decreased in number in the subgranular zone at 900 and ≥900 ppm, respectively. *Pcna* transcript level examined at 1800 ppm was decreased in the dentate gyrus. These results suggest induction of compromised cell quiescence that caused impaired self-renewal capacity of NSCs accompanying slowing down of cell cycling, which ultimately resulted in exhaustion of the NSC pool. At 1800 ppm, $Reelin^+$ hilar GABAergic interneurons were also decreased, suggesting a contribution to the NSC reduction. At this dose, $TBR2^+$ or DCX^+ progenitor and immature granule cells and $PVALB^+$ interneurons were increased. Moreover, $COX\text{-}2^+$ granule cells were increased at ≥900 ppm. These results suggest facilitation of transient progenitor cell proliferation and differentiation during exposure. Moreover, $TUNEL^+$ or Morin-stained granule cells were increased, together with *Casp12* transcript upregulation, suggesting induction of Al accumulation-related endoplasmic reticulum stress-mediated granule cell apoptosis. Transcript expression changes on cholinergic and glutamatergic signals and synaptic plasticity suggested contribution to disruptive neurogenesis. The NSC-targeting effects sustained through the adult stage despite no sustained Al-accumulation. These results suggest that developmental $AlCl_3$-exposure irreversibly affects postnatal hippocampal neurogenesis involving multiple functions in mice.

Key words: aluminum chloride; hippocampal neurogenesis; mouse; developmental neurotoxicity; synaptic plasticity.

Aluminum (Al) is the third-most abundant element found in the earth's crust and occurs naturally in the environment, foodstuffs, and drinking water (Priest, 1993). Although the concentration of Al in drinking water and foods has been low, the levels of Al in drinking water are increased by acid rain (Smith, 1996). Conversely, Al products have many modern applications. Adding

aluminum sulfate and lime to water causes aluminum hydroxide formation, which leads to settling of pollutants. Al-containing agents are also commonly found as food and medication additives. Infant formulae are especially rich in Al (Burrell and Exley, 2010). Human exposure to Al usually occurs primarily by way of the gastrointestinal tract through oral intake. In a 60-kg adult, estimated daily alimentary Al exposure is 1.6–13 mg (0.2–1.5 mg/kg body weight [BW]/week); however, relative exposure in children is higher at up to 2.3 mg/kg BW/week (EFSA, 2008).

Absorbed Al can cross the blood-brain barrier and accumulate in the brain, especially in hippocampal tissue (Struys-Ponsar *et al.*, 1997). The neurotoxic effect of Al is well known and excessive Al exposure causes multiple abnormalities of the neuronal system, especially in uremic patients with dialytic treatment, called dementia-like encephalopathy, with features similar to Alzheimer's disease (DeVoto and Yokel, 1994). In addition, mothers and their newborn infants showed nearly identical blood Al concentration in the analysis of human biological samples (Takács *et al.*, 1992), and prolonged intravenous feeding with solutions containing Al has been shown to be associated with impaired neurologic development in preterm infants (Bishop *et al.*, 1997). Experimentally, maternal Al exposure results in a high concentration of Al in the hippocampus in neonatal rats (Yuan *et al.*, 2012), and oral Al exposure during lactation has been shown to cause neurotoxicity, such as short- and long-term memory deficits in rats (Moazedi *et al.*, 2008).

The dentate gyrus in the hippocampal formation of the mammalian brain is crucial for higher brain functions, such as learning, memory, and motivation (Montaron *et al.*, 2004). During postnatal life, neurogenesis continues in the subgranular zone (SGZ) of the dentate gyrus (Zhao *et al.*, 2008). In the SGZ, type-1 neural stem cells (NSCs) differentiate into type-2a, type-2b, and type-3 progenitor cells. The type-3 cells undergo final mitosis to differentiate into immature granule cells, and then to mature granule cells (Hodge *et al.*, 2008). In the hilus of the dentate gyrus, subpopulations of γ-aminobutyric acid (GABA)-ergic interneurons innervate granule cell lineage populations to control neurogenesis in the SGZ (Masiulis *et al.*, 2011). One subpopulation of GABAergic interneurons produces Reelin, an extracellular glycoprotein that is essential for neuronal migration and correct positioning, including that for the granule cell lineage (Gong *et al.*, 2007). In addition to GABAergic neuronal inputs, various types of neurons outside the SGZ also create a synaptic connection with neurons in the dentate gyrus, such as glutamatergic neurons in the entorhinal cortex providing axonal projections to the dentate gyrus (Fonnum *et al.*, 1979) and cholinergic neurons originating from the septal nucleus and nucleus of the diagonal band of Broca innervating neurons in the hilus of the dentate gyrus (Amaral and Kurz, 1985). Glutamatergic inputs to the SGZ are important for maintaining proper proliferation and differentiation of the granule cell lineage (Freund and Buzsáki, 1996).

Recently, we reported that developmental exposure of several neurotoxicants and developmental neurotoxicants, such as manganese, acrylamide, and glycidol, targets granule cell lineages to alter a number of subpopulations during hippocampal neurogenesis (Shibutani, 2015). In addition to the changes in granule cell lineage subpopulations, we have also detected aberrations in the number of hilar GABAergic interneuron subpopulations (Shibutani, 2015). With regard to neuronal signals from outside the hippocampus to the neurons in the dentate gyrus, we also reported decreased glutamatergic or cholinergic inputs in association with disrupted neurogenesis (Itahashi *et al.*, 2015; Tanaka *et al.*, 2016). Therefore, evaluating the effects of toxicants on neurogenesis by analyzing populations of granule cell lineages in combination with interneuron subpopulations, as well as fluctuations in signal inputs, could reveal target mechanisms involved in neurogenesis.

In the present study, to determine whether exogenously administered Al targets developing nervous systems, we examined the maternal exposure effect of aluminum chloride ($AlCl_3$) on developmental neurotoxicity, targeting hippocampal neurogenesis in mouse offspring. We analyzed distribution changes of granule cell lineage subpopulations in the SGZ/GCL, as well as their cell proliferation, apoptosis and synaptic plasticity. We also analyzed distribution changes of GABAergic interneuron subpopulations in the hilus of the dentate gyrus, as well as transcript expression changes of other regulatory systems.

MATERIALS AND METHODS

Chemicals and animals. Aluminum chloride hexahydrate ($AlCl_3{\cdot}6H_2O$; purity: >98.0%; CAS No. 7784-13-6) was purchased from Wako Pure Chemical Industries, Ltd (Osaka, Japan). Thirty-six mated female Slc: ICR mice were purchased from Japan SLC, Inc (Hamamatsu, Japan) at gestational day (GD) 1 (appearance of vaginal plug was designated as GD 0). Maternal animals were individually housed in polycarbonate cages with paper bedding until postnatal day (PND) 21 (where PND 0 is the day of delivery). Animals were maintained in an air-conditioned animal room (temperature: 23 ± 2°C, relative humidity: 55 ± 15%) with a 12-h light/dark cycle. Maternal animals were allowed access to a pelleted basal diet (CRF-1; Oriental Yeast Co. Ltd, Tokyo, Japan) throughout the experimental period and distilled water (DW) *ad libitum* until the start of exposure to $AlCl_3$. From PND 21 onwards, offspring were reared with 2 or 3 animals per cage and provided with the pellet CRF-1 basal diet and DW *ad libitum*.

Experimental design. Mated female mice were randomly assigned to 3 groups of 12 animals per group by stratified randomization according to BW and treated with 0, 900, or 1800 ppm $AlCl_3$ (0, 182, or 364 ppm as Al) in DW from GD 6 to PND 21 (Supplementary Figure 1). Based on the appearance of behavioral abnormalities of mouse offspring by postnatal exposure to $AlCl_3$ during PND 1–15 via maternal drinking water at the dose level of ≥300 mg/kg body weight/day (Abu-Taweel *et al.*, 2011), a preliminary maternal exposure study, which was consisted of the dosing groups similar to or exceeding the level to induce behavioral abnormalities, ie, 0, 600, and 1200 ppm in the drinking water, was conducted ($N = 5$ dams). At 1200 ppm, male offspring exposed to $AlCl_3$ showed transient decrease in the body weight on PND 5 and female offspring decreased absolute brain weight on PND 21. There were no apparent changes in the number of live offspring and body weight of dams at both 600 and 1200 ppm. Thus, we decided to select 1800 ppm as the highest dose level that is expected to show slight maternal toxicity, according to the Organisation for Economic Co-operation and Development (OECD) guideline for the testing of chemicals (Test No. 426: Developmental Neurotoxicity Study; OECD, 2007). The lower dose was subsequently set to 900 ppm.

Body weights and food and water consumption of dams were measured twice a week throughout the experimental period. On PND 4, the litters were randomly culled to preserve 5–7 male pups and 3–5 female pups per litter. The offspring were weighed every twice a week until PND 21.

In the present study, male offspring were selected for immunohistochemical and gene expression analyses, because neurogenesis is influenced by circulating levels of steroid hormones during the estrous cycle (Pawluski *et al.*, 2009). On PND 21, 10–12

male offspring per group (1 male offspring per dam) were subjected to perfusion fixation for histopathological assessment and immunohistochemistry through the left cardiac ventricle with ice-cold 4% (w/v) paraformaldehyde (PFA) in 0.1 M phosphate buffer (pH 7.4) at a flow rate of 10 ml/min after deep anesthetization with CO_2/O_2. For gene expression analysis, 20–24 male offspring per group (2 male pups per dam) were euthanized by exsanguination from the abdominal aorta under CO_2/O_2 anesthesia and subjected to necropsy, and brains were fixed in methacarn solution at 4°C for 5 h after measuring the weight. All dams were euthanized by exsanguination from the abdominal aorta under CO_2/O_2 anesthesia and their brains were removed to fix with Bouin's solution and neutral buffered formalin (pH 7.4), respectively at 4°C overnight. Twenty-24 female offspring per group (2 female pups per dam) were also similarly euthanized for collection of brain samples to store at –20°C for other experimental purposes after measuring the weight. The remaining offspring were maintained without administration of $AlCl_3$ until PND 77, and body weight was measured once a week.

On PND 77, 10–12 male offspring per group (1 male offspring per dam) were subjected to perfusion fixation with 4% PFA buffer solution for histopathological assessment and immunohistochemistry at a flow rate of 10 ml/min. For gene expression analysis, 13–22 male offspring per group (1 or 2 male pups per dam) were euthanized by exsanguination from the abdominal aorta under CO_2/O_2 anesthesia and subjected to necropsy, and brains were fixed in methacarn solution at 4°C for 5 h after measuring the weight. Six male offspring of 1800 ppm group and 16–28 female offspring per group (1–3 female pups per dam) were also similarly euthanized for collection of brain samples to store at –20°C for other experimental purposes after measuring the weight. All animal experiments were conducted in accordance with the "Guidelines for Proper Conduct of Animal Experiments" (Science Council of Japan, June 1, 2006), and the protocols were approved by the Animal Care and Use Committee of the Tokyo University of Agriculture and Technology. All efforts were made to minimize animal suffering.

Histopathology of the brain. After fixation with 4% PFA buffer solution at PND 21 and PND 77, brains from male offspring ($N = 10$–12/group; 1 male pups per dam) were additionally immersion fixed with the same solution overnight at 4°C. Three-mm-thick coronal slices were prepared at −2.2 mm from the bregma. Brain slices were further immersion fixed with 4% PFA buffer solution overnight at 4°C and were routinely processed for paraffin embedding and sectioned into 3-μm-thick sections. Brain sections were stained with hematoxylin and eosin and subjected to histopathological examination.

Immunohistochemistry and apoptotic cell detection in the brain. Brain sections of male offspring perfused at necropsies on PND 21 and PND 77 were also subjected to immunohistochemistry using primary antibodies against proliferating cell nuclear antigen (PCNA), and the neuronal stage-defining markers, glial fibrillary acidic protein (GFAP), expressed in type-1 NSCs (radial glial cells) in the SGZ (Kempermann *et al.*, 2004), sex determining region Y-box 2 (SOX2), expressed in type-1 NSCs, type-2a and type-2b progenitor cells (Lugert *et al.*, 2012), T-box brain protein 2 (TBR2), expressed in type-2b progenitor cells in the SGZ (Lugert *et al.*, 2012), and doublecortin (DCX), expressed in type-2b and type-3 progenitor cells and immature granule cells in the SGZ and GCL (Kempermann *et al.*, 2004; Lugert *et al.*, 2012) and neuron-specific nuclear protein (NeuN), expressed in postmitotic neurons of both immature and mature granule cells in the SGZ and GCL (Kempermann *et al.*, 2004; Lugert *et al.*, 2012). Immunohistochemistry of GABAergic interneuron subpopulations was also performed using primary antibodies against Reelin, parvalbumin (PVALB), calbindin-D-28K (CALB1) and somatostatin (SST) (Freund and Buzsáki, 1996; Gong *et al.*, 2007). Immunohistochemistry of glutamatergic excitatory mossy cells was performed using primary antibody against calbindin-D-29K (CALB2; Fujise *et al.*, 1998). Immunohistochemistry of molecules related to synaptic plasticity was also performed using primary antibodies against FBL osteosarcoma oncogene (FOS), activity-regulated cytoskeleton-associated protein (ARC), and cyclooxygenase-2 (COX-2), which are the members of immediate-early genes (IEGs) involved in neuronal plasticity (Fleischmann *et al.*, 2003; Guzowski, 2002; Nahm and Noebels, 1998). Immunohistochemistry of molecules related to cell cycle was also performed using primary antibodies against $p21^{Cip1/Waf1}$, a cyclin-dependent kinase inhibitor acting in G_1/S phase (Roque *et al.*, 2012). Immunohistochemistry of molecules related to astrocyte, microglia, and oligodendrocyte was also performed using primary antibodies against GFAP, an intermediate filament expressed in astrocytes (Eng *et al.*, 2000); ionized calcium-binding adaptor molecule 1 (Iba1), a specific marker of microglia (Ito *et al.*, 1998); and oligodendrocyte transcription factor 2 (OLIG2), a specific marker of oligodendrocyte (Fang *et al.*, 2013). Incubation with the respective antibodies was performed overnight at 4°C. Primary antibodies are listed in the Supplementary Table 1. Deparaffinized sections were incubated in 0.3% hydrogen peroxide solution in absolute methanol for 30 min to quench endogenous peroxidase. Conditions of antigen retrieval applied for some antibodies were shown in Supplementary Table 1. Immunodetection was performed using a Vectastain Elite ABC kit (Vector Laboratories, Burlingame, CA) with DAB/H_2O_2 as the chromogen. Immunostained sections were then counterstained with hematoxylin and coverslipped for microscopic examination. One section per animal was subjected to each immunohistochemistry.

For evaluation of apoptosis in the SGZ or GCL of the dentate gyrus, a terminal deoxynucleotidyl transferase dUTP nick end labeling (TUNEL) assay was carried out using the ApopTag Peroxidase In situ Apoptosis Detection kit (EMD Millipore, Billerica, MA) according to the manufacturer's instructions, with DAB/H_2O_2 as the chromogen. One section per animal was subjected to TUNEL assay.

Morin (3,5,7,2′,4′-pentahydroxyflavone) staining. The Al-Morin fluorescence assay was performed for visualization and detection of Al in the SGZ/GCL, according to the protocol by Shaw and Petrik (2009). Brain sections from 5 male pups per group were stained with Morin, a fluorochrome that forms a fluorescent complex with Al fluorescing green with an excitation wavelength of 420 nm (Crapper *et al.*, 1973; De Boni *et al.*, 1974). Deparaffinized sections were first washed with phosphate buffered saline (pH 7.4) twice for 5 min, and then pretreated for 10 min in a 1% aqueous solution of hydrochloric acid, rinsed in DW twice for 5 min, and immersed in 0.2% solution of Morin (Sigma-Aldrich, St. Luis, MO) in 85% ethyl alcohol containing 0.5% acetic acid for 10 min. The sections were then washed in DW twice for 5 min, dehydrated in 70%, 90%, and 100% ethyl alcohol, cleared with 100% xylene, and mounted with Bioleit (Oken-shoji, Tokyo, Japan). One section per animal was subjected to Al-Morin fluorescence assay.

Morphometry of immunolocalized cells, apoptotic cells, and Morin-stained cells. All immunoreactive cells, ie, $GFAP^+$, $SOX2^+$, $TBR2^+$, DCX^+, $NeuN^+$, ARC^+, $COX\text{-}2^+$, FOS^+, $PCNA^+$, or $p21^{Cip1/Waf1+}$ cells, and all $TUNEL^+$ apoptotic cells in the SGZ and/or GCL of whole dentate gyrus were bilaterally counted and normalized for the entire length of the SGZ (Supplementary Figure 2). $GFAP^+$ radial glia cells were morphologically identified as those having cell bodies that reside in the SGZ and vertical processes that extend into the molecular layer of the dentate gyrus and distinguished from $GFAP^+$ astrocytes in the hilus of the hippocampal dentate gyrus. All immunoreactive cells distributed within the hilus, ie, $Reelin^+$, $PVALB^+$, $CALB1^+$, $CALB2^+$, SST^+, $NeuN^+$, $GFAP^+$, $Iba1^+$, or $OLIG2^+$ cells were bilaterally counted and normalized per unit area of the whole hilar area (Supplementary Figure 2). The immunoreactive cells were analyzed by blind trial for the treatment conditions. Cornu ammonis region 3 pyramidal neurons distributed in the hilar area were easily distinguished from hilar interneurons and excluded from counting. For quantitative measurements of each immunoreactive cellular component, digital photomicrographs at 400-fold magnification were taken using a BX53 microscope (Olympus Corp., Tokyo, Japan) attached to a DP72 Digital Camera System (Olympus Corp.), and quantitative measurements were performed using the WinROOF image analysis software package (version 5.7, Mitani Corp., Fukui, Japan).

Detection of the fluorescent complex of Morin with Al was performed as reported previously (Khan *et al.*, 2013) with some modification. To acquire Morin-fluorescence images, BX-53 fluorescence microscope (Olympus Corp.) equipped with a color charge-coupled device camera (DP72; Olympus Corp.) and cellSens imaging software (Olympus Corp.) were used. The excitation and emission filter was 400 to 440 and 460 nm (long pass), respectively. The green channel images corresponding to Morin-fluorescence were used to count the $Morin^+$ cells, following the subtraction of background of fluorescence to normalize sample-to-sample variation. All $Morin^+$ cells in the GCL of whole dentate gyrus were bilaterally counted and normalized for the entire length of the SGZ (Supplementary Figure 2).

Real-time reverse-transcription polymerase chain reaction. Real-time reverse-transcription polymerase chain reaction (RT-PCR) analysis of transcript expression in the hippocampal dentate gyrus was examined in PND 21 and PND 77 offspring. Brain tissues were dissected according to the whole-brain fixation method using methacarn solution (Akane *et al.*, 2013). In brief, 2-mm-thick coronal cerebral slices were prepared at −2.2 mm from the bregma after methacarn-fixation. Hippocampal dentate gyrus tissue was collected from the slice using a punch biopsy device with a 1-mm pore size (Kai Industries Co. Ltd, Gifu, Japan). Total RNA was extracted from tissue samples of the 0-ppm controls and 1800-ppm $AlCl_3$-exposed groups (N = 6 pups from different dams per group) using QIAzol (Qiagen, Hilden, Germany) and RNeasy Mini kit (Qiagen) according to the manufacturer's protocol. First-strand cDNA was synthesized using SuperScript III Reverse Transcriptase (Thermo Fisher Scientific, Waltham, MA) from 2 μg total RNA. Analysis of the transcript levels for gene targets shown in Supplementary Table 2 was performed with the PCR primers designed with Primer Express software (Version 3.0; Thermo Fisher Scientific). Real-time PCR with Power SYBR Green PCR Master Mix (Thermo Fisher Scientific) was conducted using individual samples (N = 6) and a StepOnePlus Real-time PCR System (Thermo Fisher Scientific). At first, comparison of the expression level was made between 0-ppm controls and 1800-ppm $AlCl_3$ group, and the relative differences in gene expression between the 2 groups were calculated with threshold cycle (C_T) values that were first normalized to those of the glyceraldehyde 3-phosphate dehydrogenase (*Gapdh*) or hypoxanthine guanine phosphoribosyl transferase (*Hprt*) gene as the endogenous control in the same sample. The relative differences in gene expression compared with control C_T values were calculated using the $2^{-\Delta\Delta C}{}_T$ method as previously described (Livak and Schmittgen, 2001).

Statistical analysis. Numerical data are presented as mean ± SD. Maternal body weights, food and water consumption, and organ weights were analyzed using the individual animal as the experimental unit. Offspring body and organ weights, immunoreactive cell counts for each antigen, and numbers of apoptotic cells were analyzed using the litter as the experimental unit. Data were analyzed using the Levene's test for homogeneity of variance. Significant differences between the 0-ppm controls and each $AlCl_3$-exposed group were evaluated as follows. If the variance was homogenous, numerical data were assessed using the Dunnett's test. For heterogeneous data, the Aspin-Welch's *t*-test with Bonferroni correction was applied. Numerical data consisting of 2 sample groups were analyzed using the Student's *t*-test when the variance was homogenous between the groups, and the Aspin-Welch's *t*-test was performed when data were heterogeneous. All analyses were performed using the IBM SPSS Statistics ver. 25 (IBM Japan, Ltd, Tokyo, Japan).

RESULTS

Maternal Parameters

One nonpregnant animal in the 900-ppm group and 2 animals which had abortions, one each in the 900-ppm and 1800-ppm group, as confirmed by examination of implantation sites and the number of live offspring at birth, were excluded from the experiment. Therefore, effective number of dams were 12, 10, and 11 for 0-, 900-, and 1800-ppm group, respectively. The number of implantation sites and live offspring and male ratio were not different between the 0-ppm controls and the $AlCl_3$-exposed groups (Supplementary Table 3). Dams showed no significant changes in body weight during gestation and lactation periods between the 0-ppm and any of the exposed groups (Figure 1). Food consumption was significantly decreased on PND 2 in the 900- and 1800-ppm groups and on PND 19 in the 1800-ppm group compared with 0-ppm controls (Figure 1). Water consumption was significantly decreased from PND 9 to PND 21 in the 900-ppm group, and from GD 17 to PND 21 in the 1800-ppm group, compared with 0-ppm controls (Figure 1). There were no abnormalities in the gait and behaviors of dams in any group. At necropsy on PND 21, there were no change in absolute and relative brain weights in any group (Supplementary Table 3). Based on mean values of water consumption, dams in the 900- and 1800-ppm groups received 107.9 and 207.1 mg/kg body weight/day Al, respectively, during the gestation period. Dams took 319.8 and 574.5 mg/kg body weight/day Al during the lactation period, respectively.

Clinical Observation and Necropsy Data of Offspring

No abnormalities in the gait and behaviors were observed in offspring of any group before necropsy on PND 21 and after weaning. Body weights of male offspring of the 1800-ppm group

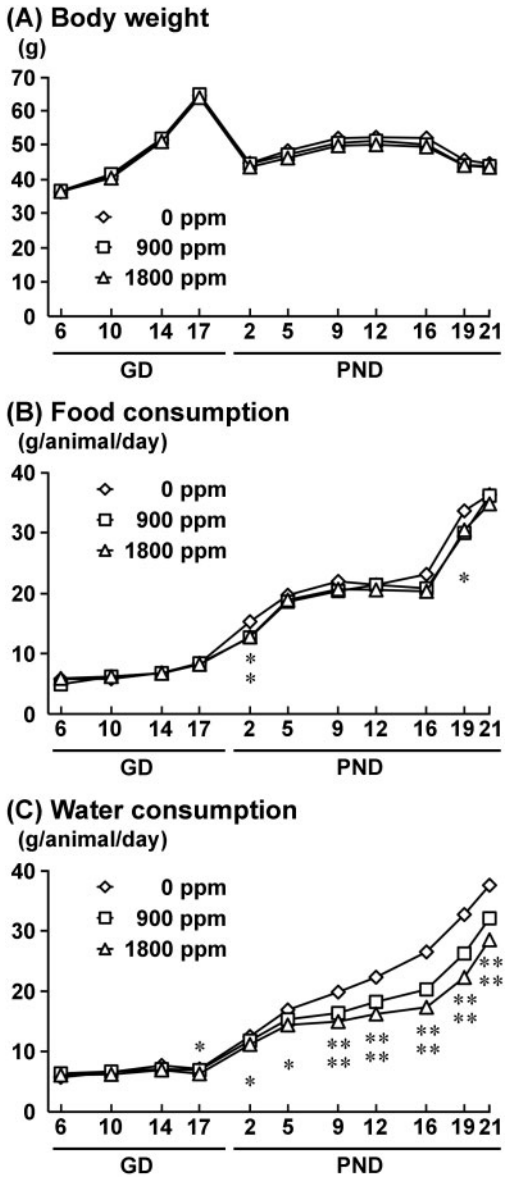

Figure 1. Body weight (A), food consumption (B), and water consumption (C) of dams during the exposure period. $^{*}p < .05$, $^{**}p < .01$, compared with the 0-ppm controls by Dunnett's test or Aspin-Welch's *t*-test with Bonferroni correction.

significantly decreased from PND 4 to PND 77 compared with 0-ppm controls. Body weights of female offspring of the 900-ppm group from PND 4 to PND 12 and from PND 19 to PND 35 and of the 1800-ppm group from PND 4 to PND 56 significantly decreased compared with 0-ppm controls (Supplementary Table 4). At necropsy on PND 21, male offspring of the 1800-ppm group and female offspring of the 900- and 1800-ppm groups showed significantly decreased body weight compared with 0-ppm controls (Table 1). At necropsy on PND 77, male offspring of the 1800-ppm group showed significantly decreased body weight compared with 0-ppm controls. With regard to brain weight in male offspring on PND 21, relative weight was significantly higher in the 1800-ppm group compared with 0-ppm controls (Table 1). In female offspring, absolute weight was significantly lower in the 1800-ppm group and relative weight was significantly higher in the 900- and 1800-ppm groups, compared with 0-ppm controls. With regard to brain weight in male offspring on PND 77, absolute and relative weights showed no change in any group. In female offspring, absolute brain weight was significantly lower in the 1800-ppm group compared with 0-ppm controls.

Brain Histopathology of Male Offspring

There were no histopathological changes in the brain of male offspring in any group at both PND 21 and PND 77.

Distribution of Granule Cell Lineage Subpopulations in the SGZ and GCL of Male Offspring

On PND 21, the number of $GFAP^+$ cells in the SGZ was significantly less at 900 ppm, and the number of $TBR2^+$ cells in the SGZ and DCX^+ cells in the SGZ/GCL was significantly greater at 1800 ppm compared with 0-ppm controls (Figure 2). With regard to $SOX2^+$ cells in the SGZ and $NeuN^+$ cells in the GCL, there were no significant differences in any exposure group compared with 0-ppm controls. On PND 77, the number of $GFAP^+$ cells in the SGZ was significantly less at 1800 ppm (Figure 2 and Supplementary Figure 3). However, no significant differences were observed in the number of $SOX2^+$ cells and $TBR2^+$ cells in the SGZ, and DCX^+ cells in the SGZ/GCL, and $NeuN^+$ cells in the GCL of any exposure group compared with 0-ppm controls.

Distribution of Neuronal Subpopulations in the Hilus of the Dentate Gyrus of Male Offspring

On PND 21, the number of $Reelin^+$ cells in the hilus was significantly less at 1800 ppm compared with 0-ppm controls, and the number of $PVALB^+$ cells was significantly greater at 1800 ppm compared with 0-ppm controls (Figure 3). There were no significant differences in the number of $CALB1^+$ cells, $CALB2^+$ cells and SST^+ cells and $NeuN^+$ postmitotic neurons of any exposure group compared with 0-ppm controls (Figure 3 and Supplementary Figures 4 and 5). On PND 77, the number of $Reelin^+$ cells was significantly less at ≥900 ppm compared with 0-ppm controls (Figure 3 and Supplementary Figure 6). No significant differences were observed in the numbers of $PVALB^+$ cells, $CALB1^+$ cells, $CALB2^+$ cells, SST^+ cells and $NeuN^+$ mature neurons of any exposure group compared with 0-ppm controls (Figure 3 and Supplementary Figures 4–6).

Proliferating, Apoptotic and Cycle-Arrested Cells in the SGZ and GCL of Male Offspring

On PND 21, there was no significant difference in the number of $PCNA^+$ proliferating cells and $TUNEL^+$ apoptotic cells in the SGZ in any exposure group compared with 0-ppm controls (Figure 4). On the other hand, the number of $TUNEL^+$ apoptotic cells in the GCL was significantly greater at 900 ppm compared with 0-ppm controls. The number of $p21^{Cip1/Waf1+}$ cells in the SGZ was significantly less at ≥900 ppm compared with 0-ppm controls. On PND 77, no significant differences were observed in the number of $PCNA^+$ cells in the SGZ, $TUNEL^+$ cells in the SGZ or GCL and $p21^{Cip1/Waf1+}$ cells in the SGZ in any exposure group compared with 0-ppm controls (Figure 4 and Supplementary Figure 7).

Distribution of Synaptic Plasticity-Related Molecules in the GCL of Male Offspring

On PND 21, the number of $COX\text{-}2^+$ cells in the GCL was significantly greater at ≥900 ppm compared with 0-ppm controls, whereas there were no significant differences in the numbers of ARC^+ cells and FOS^+ cells in any exposure group compared with 0-ppm controls (Figure 5). On PND 77, no significant differences were observed in the numbers of FOS^+ cells, ARC^+ cells and

Table 1. Body and Brain Weights of Offspring on PND 21 and PND 77

	$AlCl_3$ in Drinking Water (ppm)		
	0 (Control)	900	1800
PND 21			
Males			
No. of offspring examined	36	30	33
Body weight (g)	17.9 ± 0.9	16.9 ± 1.3	15.6 ± 0.8**
No. of offspring examined	24	20	22
Brain weight (g)	0.45 ± 0.02	0.44 ± 0.01	0.43 ± 0.01
(g/100g body weight)	2.50 ± 0.15	2.65 ± 0.26	2.79 ± 0.18**
Females			
No. of offspring examined	24	20	22
Body weight (g)	17.4 ± 0.7	15.7 ± 1.5**	15.1 ± 0.7**
Brain weight (g)	0.44 ± 0.01	0.43 ± 0.01	0.43 ± 0.02*
(g/100g body weight)	2.58 ± 0.19	2.82 ± 0.24*	2.90 ± 0.13**
PND 77			
Males			
No. of offspring examined	32	23	39
Body weight (g)	53.0 ± 2.8	53.0 ± 4.7	48.3 ± 2.1**
No. of offspring examined	20	13	28
Brain weight (g)	0.50 ± 0.01	0.50 ± 0.02	0.50 ± 0.02
(g/100g body weight)	0.98 ± 0.08	0.94 ± 0.10	1.04 ± 0.08
Females			
No. of offspring examined	28	27	16
Body weight (g)	42.5 ± 4.4	43.7 ± 2.7	40.5 ± 3.4
Brain weight (g)	0.51 ± 0.02	0.49 ± 0.02	0.48 ± 0.03*
(g/100g body weight)	1.85 ± 0.08	1.89 ± 0.09	1.95 ± 0.17

Abbreviations: PND, postnatal day; $AlCl_3$, aluminum chloride.
Data are expressed as the mean ± SD.
*$p < .05$,
**$p < .01$, compared with the 0-ppm controls by Dunnett's test or Aspin-Welch's t-test with Bonferroni correction.

$COX\text{-}2^+$ cells in any exposure group compared with 0-ppm controls (Figure 5 and Supplementary Figure 8).

Morin$^+$ Cells in the SGZ/GCL of Male Offspring

On PND 21, $Morin^+$ cells were observed in the GCL in addition to the SGZ in $AlCl_3$-exposed offspring, whereas $Morin^+$ cells were observed mainly in the SGZ in 0-ppm controls (Figure 6). The number of $Morin^+$ cells was significantly higher at ≥900 ppm compared with 0-ppm controls. On PND 77, no significant differences in the number of $Morin^+$ cells were observed in any exposure group compared with 0-ppm controls (Figure 6).

Distribution of Astrocytes, Microglia and Oligodendrocytes in the Hilus of the Dentate Gyrus of Male Offspring

On PND 21, there were no significant differences in the numbers of $GFAP^+$ cells, $Iba1^+$ cells and $OLIG2^+$ cells in the hilus of any exposure group compared with 0-ppm controls (Supplementary Figures 9 and 10). On PND 77, the number of $Iba1^+$ cells was significantly greater at 900 ppm compared with 0-ppm controls (Supplementary Figures 9 and 10). No significant differences were observed in the number of $GFAP^+$ cells and $OLIG2^+$ cells of any exposure group compared with 0-ppm controls.

Transcript Expression Changes in the Dentate Gyrus of Male Offspring

Transcript expression level was compared between 0-ppm controls and 1800-ppm group on PND 21 and PND 77 (Table 2). With regard to synaptic plasticity-related genes, expression level of *Arc* significantly increased after normalization with *Hprt* at 1800 ppm compared with 0-ppm controls on PND 21 and decreased after normalization with *Gapdh* and *Hprt* at 1800 ppm compared with 0-ppm controls on PND 77. With regard to cell proliferation-related *Pcna*, expression level significantly decreased after normalization with *Gapdh* and *Hprt* at 1800 ppm compared with 0-ppm controls on PND 21 and with *Gapdh* at 1800 ppm compared with 0-ppm controls on PND 77. With regard to cholinergic receptor genes, transcript expression levels of *Chrna4* significantly decreased after normalization with *Gapdh* at 1800 ppm compared with 0-ppm controls on PND 21. With regard to genes of glutamate transporters and receptors, expression level of *Slc17a6* significantly decreased after normalization with *Gapdh* and *Hprt* at 1800 ppm compared with 0-ppm controls on PND 21 and increased after normalization with *Hprt* at 1800 ppm compared with 0-ppm controls on PND 77. Expression levels of *Gria3* and *Grin2a* significantly increased after normalization with *Hprt* at 1800 ppm compared with 0-ppm controls on PND 21. In contrast, *Grin2d* expression levels significantly decreased after normalization with *Gapdh* at 1800 ppm compared with 0-ppm controls on PND 21 and increased after normalization with *Hprt* at 1800 ppm compared with 0-ppm controls on PND 77. With regard to apoptosis-related genes, expression level of *Bax* significantly decreased after normalization with *Gapdh* at 1800 ppm compared with 0-ppm controls on PND 21 and PND 77. Expression level of *Casp12* significantly increased after normalization with *Hprt* at 1800 ppm compared with 0-ppm controls on PND 21. Expression level of *Casp2* significantly increased after normalization with *Hprt* at 1800 ppm compared with 0-ppm controls on PND 77. Other genes listed in Table 2 did not show significant fluctuations in transcript expression levels between 0-ppm controls and the 1800-ppm group on both PND 21 and PND 77.

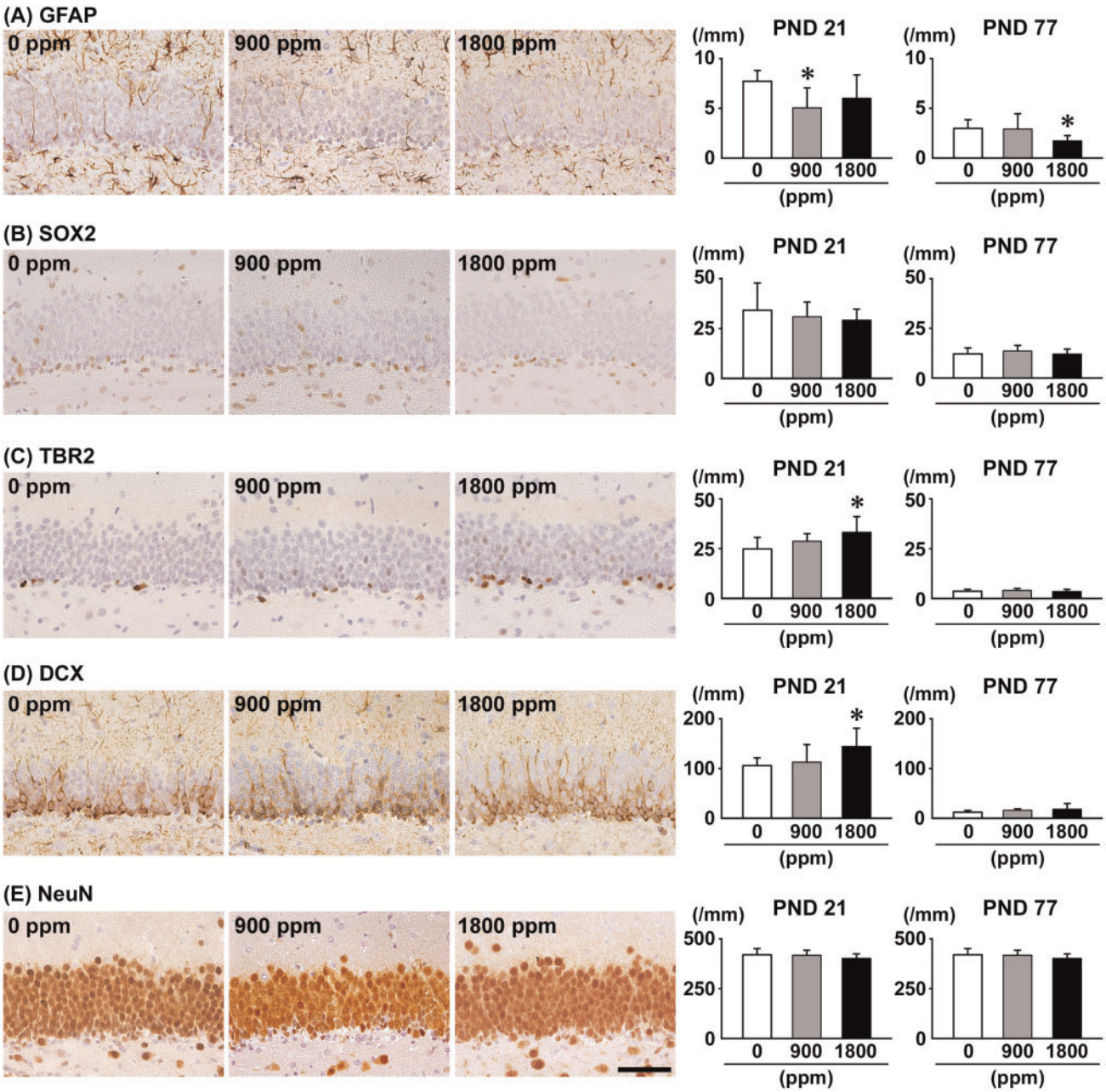

Figure 2. Distribution of immunoreactive cells for (A) glial fibrillary acidic protein (GFAP), (B) SRY (sex determining region Y)-box2 (SOX2), and (C) T box brain protein 2 (TBR2) in the subgranular zone (SGZ), (D) doublecortin (DCX) in the SGZ and granule cell layer (GCL), and (E) neuron-specific nuclear protein (NeuN) in the GCL of male offspring at postnatal day (PND) 21 and PND 77 after maternal exposure to aluminum chloride ($AlCL_3$) from gestational day (GD) 6 to PND 21. Representative images from the 0-ppm controls (left), and the 900-ppm (middle), and 1800-ppm (right) $AlCL_3$ groups at PND 21. Magnification ×400; bar 50 μm. Graphs show the numbers of immunoreactive cells in the SGZ and/or GCL. $N = 9$–12/group (PND 21: 0-ppm controls, 10; 900-ppm $AlCL_3$, 10; 1800-ppm $AlCL_3$, 10; PND 77: 0-ppm controls, 12; 900-ppm $AlCL_3$, 9; 1800-ppm $AlCL_3$, 11). *$p < .05$, compared with the 0-ppm controls by Dunnett's test or Aspin-Welch's t-test with Bonferroni correction.

DISCUSSION

In the present study, we observed decreases of $GFAP^+$ type-1 NSCs at 900 ppm and $p21^{Cip1/Waf1+}$ SGZ cells at ≥900 ppm and hilar $Reelin^+$ cells at 1800 ppm on PND 21. We also observed statistically non-significant decrease of $GFAP^+$ type-1 NSCs at 1800 ppm. The $p21^{Cip1/Waf1}$ induces cell cycle arrest at the G_1/S checkpoint to maintain relative quiescence (Roque *et al.*, 2012). The loss of $p21^{Cip1/Waf1}$ expression increases NSC proliferation by compromising cell quiescence, especially under stress conditions (Kippin *et al.*, 2005; Qiu *et al.*, 2004). Then, the loss of $p21^{Cip1/Waf1}$ expression leads to self-renewal exhaustion and progressive decline in NSC proliferation rate by slowing down of cell cycling (Kippin *et al.*, 2005). In addition, Reelin-deficiency in reeler mice causes decreased proliferation of NSCs in the hippocampus, suggesting that Reelin functions to maintain NSC proliferation (Sibbe *et al.*, 2015). Therefore, it may be possible to consider that $AlCl_3$ causes $p21^{Cip1/Waf1}$ downregulation to trigger a reduction of the NSC pool, and then downregulation of Reelin in interneurons to weaken NSC proliferation at the developmental stage. We also found *Pcna* transcript downregulation at 1800 ppm on PND 21, suggesting that $AlCl_3$ exposure leads to

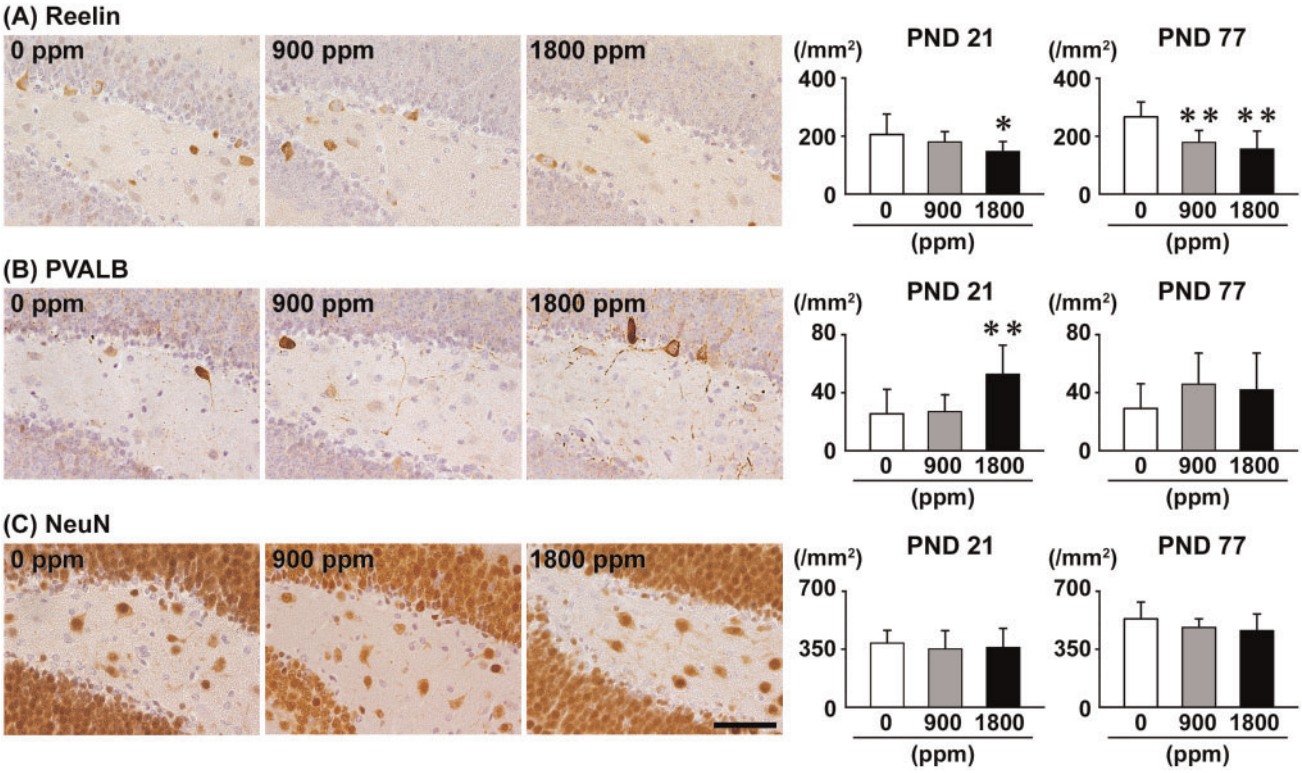

Figure 3. Distribution of interneurons immunoreactive for (A) Reelin or (B) parvalbumin (PVALB), and (C) NeuN-immunoreactive postmitotic neurons in the hilus of the hippocampal dentate gyrus of male offspring at PND 21 and PND 77 after maternal exposure to aluminum chloride ($AlCl_3$) from GD 6 to PND 21. Representative images from the 0-ppm controls (left) and the 900-ppm (middle) and 1800-ppm (right) $AlCl_3$ groups at PND 21. Magnification ×400; bar 50 μm. Graphs show the numbers of immunoreactive interneurons in the hilus. $N = 9$–12/group (PND 21: 0-ppm controls, 10; 900-ppm $AlCl_3$, 10; 1800-ppm $AlCl_3$, 10; PND 77: 0-ppm controls, 12; 900-ppm $AlCl_3$, 9; 1800-ppm $AlCl_3$, 11). *$p < .05$, **$p < .01$, compared with the 0-ppm controls by Dunnett's test or Aspin-Welch's *t*-test with Bonferroni correction.

NSCs slowing down cell cycling. Importantly, decreases of $GFAP^+$ NSCs, *Pcna* transcript level, and $Reelin^+$ cells were sustained through the adult stage on PND 77. We also observed a tendency to decrease $p21^{Cip1/Waf1+}$ cells on PND 77. These results suggest an irreversible effect on hippocampal neurogenesis by developmental $AlCl_3$ exposure.

In the present study, we observed increases of $TBR2^+$ and DCX^+ cells, reflecting increase of type-2 and type-3 progenitor cells and immature granule cells, in the SGZ/GCL, and also increase of hilar $PVALB^+$ cells at 1800 ppm on PND 21. $PVALB^+$ GABAergic interneurons have been shown to promote differentiation of type-2 progenitor cells (Freund and Buzsáki, 1996; Tozuka *et al.*, 2005), suggesting an increase of $PVALB^+$ interneuron signals to cause an increase of $TBR2^+$ and DCX^+ cells. We also found transcript upregulation of *Grin2a*, which encodes one of the *N*-methyl-D-aspartate receptor (NMDAR) subunits, ie, NR2A, at 1800 ppm on PND 21. NR2A is essential to maintaining PVALB expression in GABAergic interneurons (Kinney *et al.*, 2006), suggesting that *Grin2a* transcript upregulation is evidence for increase of $PVALB^+$ interneurons. We further observed an increase of GCL $COX\text{-}2^+$ cells at ≥900 ppm on PND 21. Reportedly, COX-2 in mature granule cells activates cell proliferation by producing prostaglandin E2/EP2 signals in SGZ progenitor cells (Ma *et al.*, 2017). Moreover, *Ptgs2* knockout mice have decreased DCX^+ cells (Nam *et al.*, 2015). Therefore, the increase of GCL $COX\text{-}2^+$ cells observed here may cause an increase of progenitor cells during $AlCl_3$ exposure. However, transcript levels of *Pcna* were decreased at the end of exposure, suggestive of the suppression of progenitor cell proliferation to adjust excessive progenitor cell proliferation at the developmental stage.

In the present study, we did not observe any change in the number of $NeuN^+$ mature granule cells by developmental $AlCl_3$ exposure, despite the increases of type-2b, type-3 and immature cells in the SGZ/GCL at 1800 ppm on PND 21. However, $TUNEL^+$ apoptotic granule cells were increased at ≥900 ppm on PND 21, whereas the increase was statistically insignificant at 1800 ppm. Therefore, a balance between the increases of the progenitor and immature granule cell population and loss of granule cells by apoptosis may result in an unchanged number of GCL $NeuN^+$ cells on PND 21 by $AlCl_3$-exposure. Conversely, we observed downregulation of *Bax*, a Bcl-2 family gene that is able to initiate the intrinsic apoptosis pathway (Gross *et al.*, 1998), examined at 1800 ppm on PND 21. In contrast, we observed transcript upregulation of *Casp12* at 1800 ppm. Considering the crucial role of caspase 12 in the progression of endoplasmic reticulum (ER) stress-mediated apoptosis (Yoneda *et al.*, 2001), facilitation of ER stress-mediated apoptosis and suppression of the intrinsic pathway of apoptosis may result in a nonsignificant increase of granule cell apoptosis at 1800 ppm. Interestingly, Al-accumulated granule cells as evident by Morin-staining were dose-dependently increased at ≥900 ppm on PND 21. Neuronal cell apoptosis has been suggested in relation with their Al accumulation (Abdel Moneim, 2012; Shaw and Petrik, 2009). Because Al can induce ER stress-mediated apoptosis (Mustafa Rizvi *et al.*, 2014), an increase of granule cell apoptosis at ≥900 ppm may be related to the cytotoxic effect of accumulated Al in granule cells in the present study. At 1800 ppm, a protective mechanism, such as suppression of the BAX-mediated intrinsic pathway of apoptosis, may be predominated. On PND 77, $AlCl_3$-exposed animals did not see an increase in Al-accumulated cells and

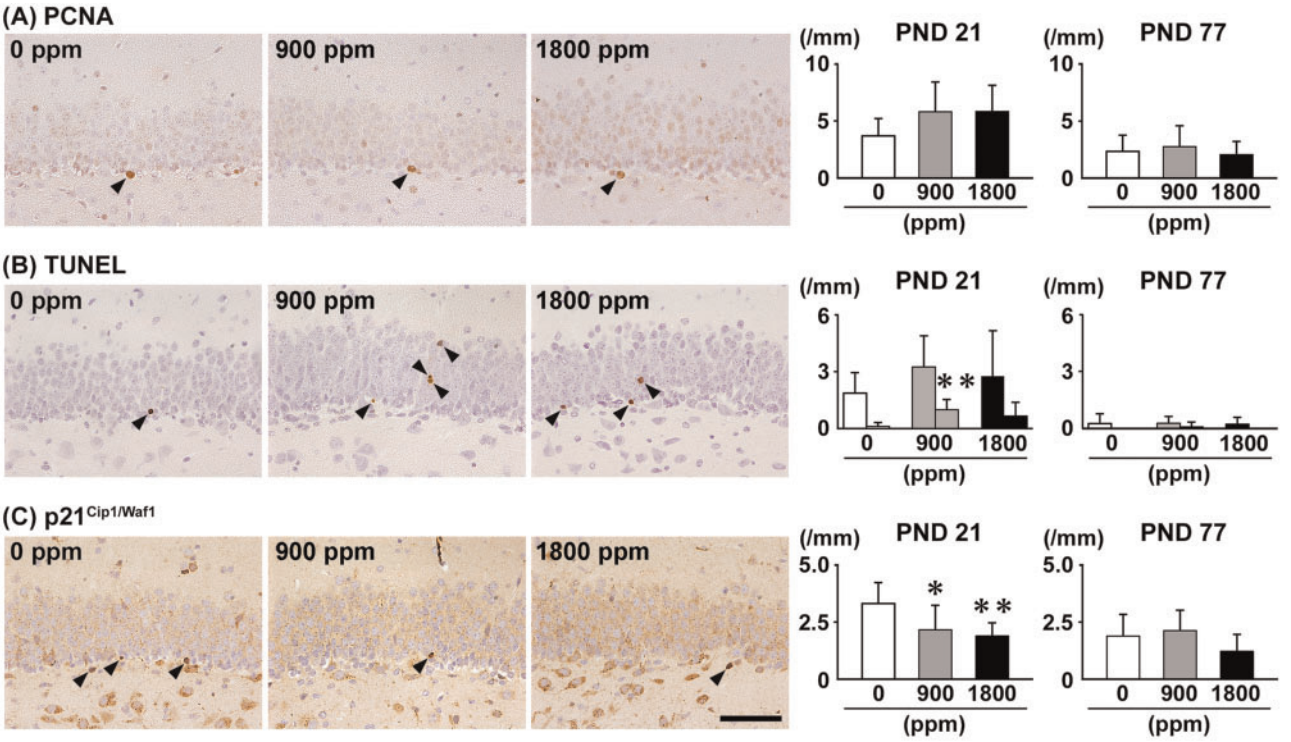

Figure 4. Distribution of (A) proliferating cell nuclear antigen (PCNA)$^+$ proliferating cells in the SGZ, (B) terminal deoxynucleotidyl transferase dUTP nick end labeling (TUNEL)$^+$ apoptotic cells in the SGZ or the GCL, and (C) p21$^{Cip1/Waf1+}$ cells in the SGZ of male offspring at PND 21 and PND 77 after maternal exposure to aluminum chloride ($AlCl_3$) from GD 6 to PND 21. Representative images from the 0-ppm controls (left) and the 900-ppm (middle) and 1800-ppm (right) $AlCl_3$ groups at PND 21. Arrowheads indicate immunoreactive or TUNEL$^+$ apoptotic cells. Magnification ×400; bar 50 μm. Graphs show the numbers of immunoreactive cells in the SGZ or GCL. In the graphs of (B), left and right columns at each dose indicate the numbers of TUNEL$^+$ cells in the SGZ and in the GCL, respectively. $N = 9$–12/group (PND 21: 0-ppm controls, 10; 900-ppm $AlCl_3$, 10; 1800-ppm $AlCl_3$, 10; PND 77: 0-ppm controls, 12; 900-ppm $AlCl_3$, 9; 1800-ppm $AlCl_3$, 11). $^*p < .05$, $^{**}p < .01$, compared with the 0-ppm controls by Dunnett's test or Aspin-Welch's *t*-test with Bonferroni correction.

apoptosis in the SGZ/GCL. Considering the functional role of *Casp2* as a potent activator of the downstream intrinsic pathway of apoptosis, downregulation of *Bax*, irrespective of the upregulation of *Casp2*, suggested suppression of the intrinsic pathway of apoptosis at the adult stage. Detection of Morin$^+$ cells in the SGZ of all groups including 0-ppm controls in the present study may be the reflection of basal Al accumulation in the brain of normal animals (Baydar *et al.*, 2003).

In the present study, we observed transcript downregulation of *Grin2d* and *Chrna4* on PND 21 at 1800 ppm. GRIN2D is a subunit protein of NMDA receptors and CHRNA4 is a subunit of the neuronal nicotinic acetylcholine receptor, both being expressed in GABAergic interneurons (Son and Winzer-Serhan, 2008; Yamasaki *et al.*, 2014), suggesting an involvement of both glutamatergic and cholinergic signals in GABAergic interneurons to indirectly affect neurogenesis. In contrast, *Grin2d* transcript level was increased on PND 77, probably reflecting a compensatory response against downregulation on PND 21. Although the functional involvement of CHRNA4 in the hippocampal neurogenesis is not reported, CHRNB2 has been shown to play an important role in regulating SGZ cell proliferation (Harrist *et al.*, 2004). Therefore, the decreased CHRNA4 subunit may affect tetramerization involving CHRNB2 to cause downregulation of the nicotinic acetylcholine receptor in GABAergic interneurons at 1800 ppm on PND 21, resulting in insufficient inputs from hilar GABAergic interneurons to the SGZ.

Synaptic plasticity in the hippocampus as a cellular mechanism of learning and memory requires appropriate integration of glutamatergic excitatory and GABAergic inhibitory synaptic inputs (Bliss and Collingridge, 1993). In the present study, we observed transcript upregulation of *Arc* at 1800 ppm on PND 21. ARC is a member of the IEGs that play a role in the initial steps of neuronal plasticity including axonal and synaptic plasticities (Guzowski, 2002). However, *Arc* transcript level turned to be suppressed on PND 77, suggestive of suppression of ARC-related synaptic plasticity. Interestingly, NMDA receptor activation upregulates ARC expression (Alaghband *et al.*, 2014). As aforementioned, $AlCl_3$ exposure upregulated transcript of the glutamatergic receptor subunit of NR2A at 1800 ppm on PND 21, suggesting a relation to the transcript upregulation of *Arc* for increase of GCL synaptic plasticity.

In the present study, we found transcript upregulation of *Gria3* at 1800 ppm on PND 21. GRIA3, a subunit of alpha-amino-3-hydroxy-5-methyl-4-isoxazolepropionic acid receptor (AMPAR), is reportedly found at excitatory synapses throughout the brain (Ozawa *et al.*, 1998). The cellular models of synaptic plasticity, especially of long-term potentiation, can be expressed by the synaptic insertion of AMPARs (Kessels and Malinow, 2009). Conversely, ARC interacts with endocytic machinery to regulate AMPAR trafficking and contributes to late-phase synaptic plasticity and memory consolidation (Chowdhury *et al.*, 2006). These results suggest that transcript upregulation of *Arc* may facilitate membrane trafficking of increased GRIA3 on PND 21 by developmental $AlCl_3$ exposure, whereas the ARC$^+$ granule cells did not fluctuate in number. COX-2 is another molecule regulating synaptic plasticity of GCL (Chen *et al.*, 2002), and the number of COX-2$^+$ granule cells was increased at ≥900 ppm on PND 21 in the present study,

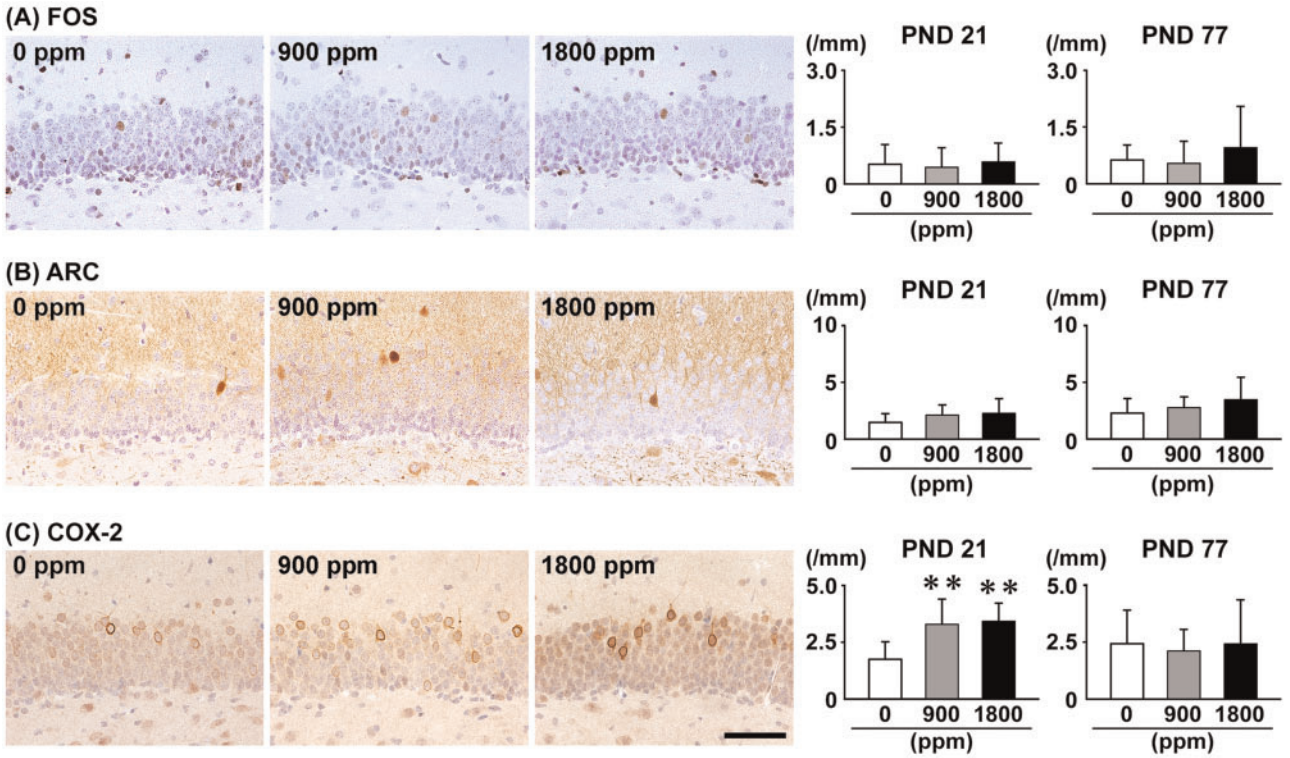

Figure 5. Distribution of immunoreactive cells for (A) FBJ osteosarcoma oncogene (FOS), (B) activity-regulated cytoskeleton-associated protein (ARC), and (C) cyclooxygenase-2 (COX-2) in the GCL of the hippocampal dentate gyrus of male offspring at PND 21 and PND 77 after maternal exposure to aluminum chloride ($AlCl_3$) from GD 6 to PND 21. Representative images from the 0-ppm controls (left) and the 900-ppm (middle) and 1800-ppm (right) $AlCl_3$ groups at PND 21. Magnification ×400; bar 50 μm. Graphs show the numbers of immunoreactive cells in the GCL. $N = 9$–12/group (PND 21: 0-ppm controls, 10; 900-ppm $AlCl_3$, 10; 1800-ppm $AlCl_3$, 10; PND 77: 0-ppm controls, 12; 900-ppm $AlCl_3$, 9; 1800-ppm $AlCl_3$, 11). $^{**}p < .01$, compared with the 0-ppm controls by Dunnett's test or Aspin-Welch's *t*-test with Bonferroni correction.

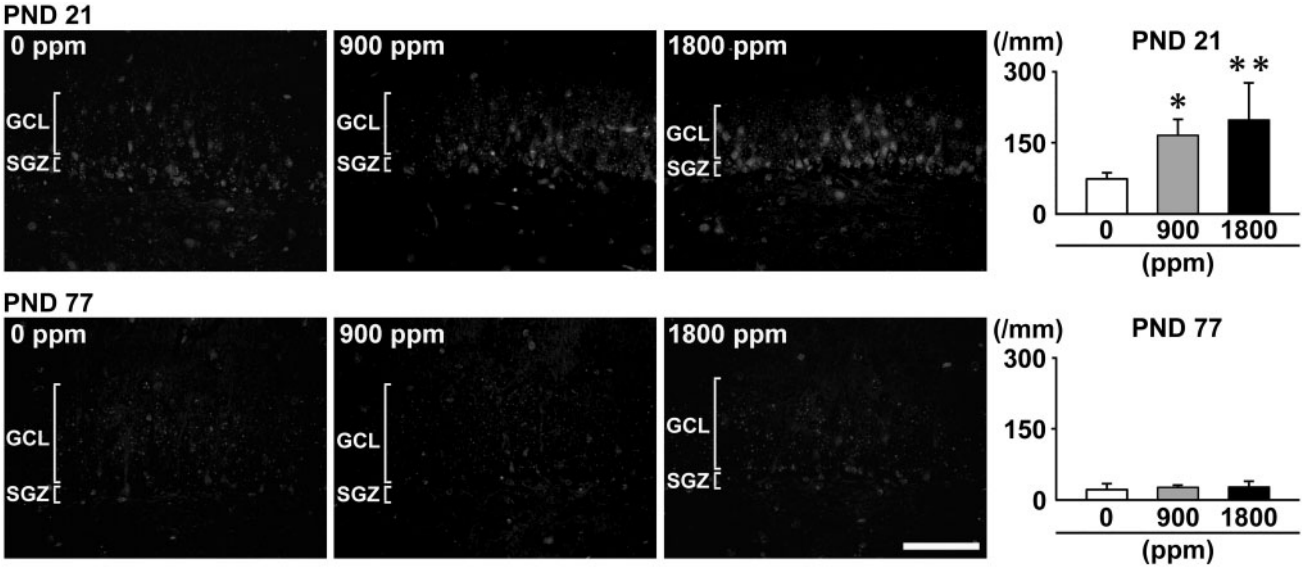

Figure 6. Distribution of Morin$^+$ cells in the SGZ/GCL of the hippocampal dentate gyrus of male offspring at PND 21 and PND 77 after maternal exposure to aluminum chloride ($AlCl_3$) from GD 6 to PND 21. Representative images from the 0-ppm controls (left) and the 900-ppm (middle) and 1800-ppm (right) $AlCl_3$ groups at PND 21. Magnification ×400; bar 50 μm. Graphs show the numbers of Morin$^+$ cells in the GCL. $N = 5$/group. $^{*}p < .05$, $^{**}p < .01$, compared with the 0-ppm controls by Dunnett's test or Aspin-Welch's *t*-test with Bonferroni correction.

Table 2. Real-time RT-PCR Analysis Data in the Hippocampal Dentate Gyrus on PND 21 and PND 77

	0 ppm $AlCl_3$ (Control)		1800 ppm $AlCl_3$	
	Relative Transcript Level Normalized to		Relative Transcript Level Normalized to	
	Gapdh	*Hprt*	*Gapdh*	*Hprt*
No. of animals examined[a]	6	6	6	6
PND 21				
Synaptic plasticity				
Arc	1.02 ± 0.23	1.04 ± 0.32	1.63 ± 0.87	1.83 ± 0.80*
Ptgs2	1.02 ± 0.24	1.01 ± 0.13	0.78 ± 0.15	0.89 ± 0.10
Fos	1.02 ± 0.21	1.02 ± 0.24	0.98 ± 0.31	1.14 ± 0.38
Stem cell regulation				
Kitl	1.02 ± 0.25	1.04 ± 0.32	0.78 ± 0.19	1.02 ± 0.37
Notch1	1.03 ± 0.28	1.07 ± 0.42	0.89 ± 0.29	1.14 ± 0.43
Cell proliferation				
Pcna	1.01 ± 0.15	1.00 ± 0.06	0.71 ± 0.15**	0.81 ± 0.12**
Neurotrophic action				
Ntrk2	1.03 ± 0.29	1.09 ± 0.52	0.98 ± 0.19	1.29 ± 0.45
Bdnf	1.07 ± 0.42	1.08 ± 0.48	1.21 ± 0.28	1.60 ± 0.60
Cholinergic receptors				
Chrna7	1.03 ± 0.30	1.04 ± 0.34	1.13 ± 0.39	1.29 ± 0.35
Chrna4	1.01 ± 0.17	1.07 ± 0.43	0.66 ± 0.25*	0.82 ± 0.28
Chrnb2	1.02 ± 0.20	1.02 ± 0.20	0.82 ± 0.11	0.95 ± 0.13
Glutamate transporters/receptors				
Slc17a6	1.05 ± 0.41	1.05 ± 0.37	0.47 ± 0.22*	0.58 ± 0.21*
Slc17a7	1.12 ± 0.63	1.15 ± 0.76	1.94 ± 0.97	2.19 ± 0.89
Gria1	1.09 ± 0.53	1.10 ± 0.48	1.12 ± 0.28	1.44 ± 0.47
Gria2	1.10 ± 0.50	1.09 ± 0.53	1.52 ± 0.59	2.00 ± 0.93
Gria3	1.03 ± 0.25	1.02 ± 0.22	1.37 ± 0.44	1.56 ± 0.39*
Grin2a	1.07 ± 0.41	1.07 ± 0.45	1.77 ± 0.69	2.36 ± 1.13*
Grin2d	1.02 ± 0.24	1.11 ± 0.52	0.55 ± 0.14**	0.70 ± 0.15
Apoptosis				
Bax	1.01 ± 0.18	1.01 ± 0.11	0.78 ± 0.13*	0.89 ± 0.09
Bcl2	1.02 ± 0.20	1.00 ± 0.08	1.06 ± 0.32	1.22 ± 0.30
Casp2	1.01 ± 0.17	1.02 ± 0.22	1.02 ± 0.23	1.16 ± 0.17
Casp3	1.04 ± 0.28	1.04 ± 0.31	0.97 ± 0.12	1.27 ± 0.36
Casp9	1.02 ± 0.18	1.01 ± 0.16	0.95 ± 0.16	1.09 ± 0.14
Casp12	1.02 ± 0.20	1.02 ± 0.21	1.21 ± 0.28	1.38 ± 0.22*
PND 77				
Synaptic plasticity				
Arc	1.02 ± 0.21	1.01 ± 0.18	0.36 ± 0.14**	0.45 ± 0.15**
Ptgs2	1.06 ± 0.44	1.01 ± 0.18	0.79 ± 0.38	0.96 ± 0.25
Fos	1.01 ± 0.12	1.02 ± 0.18	0.79 ± 0.31	0.98 ± 0.18
Stem cell regulation				
Kitl	1.14 ± 0.54	1.33 ± 0.55	1.49 ± 0.92	1.74 ± 0.80
Notch1	1.02 ± 0.24	1.01 ± 0.35	0.91 ± 0.35	1.14 ± 0.22
Cell proliferation				
Pcna	1.02 ± 0.20	1.01 ± 0.16	0.72 ± 0.22*	0.92 ± 0.15
Neurotrophic action				
Ntrk2	1.02 ± 0.26	1.00 ± 0.09	0.86 ± 0.34	1.07 ± 0.17
Bdnf	1.05 ± 0.39	1.04 ± 0.29	0.92 ± 0.26	1.17 ± 0.10
Cholinergic transporters/receptors				
Chrna7	1.07 ± 0.48	1.04 ± 0.32	0.89 ± 0.27	1.13 ± 0.17
Chrna4	1.13 ± 0.60	1.13 ± 0.58	1.45 ± 0.71	1.75 ± 0.45
Chrnb2	1.04 ± 0.30	1.03 ± 0.30	1.10 ± 0.49	1.34 ± 0.28
Glutamate receptors				
Slc17a6	1.26 ± 0.82	1.26 ± 0.87	2.37 ± 1.35	2.82 ± 0.98*
Slc17a7	1.11 ± 0.62	1.06 ± 0.39	0.79 ± 0.16	1.03 ± 0.10
Gria1	1.07 ± 0.47	1.04 ± 0.30	1.02 ± 0.28	1.31 ± 0.15
Gria2	1.04 ± 0.33	1.03 ± 0.26	0.81 ± 0.19	1.05 ± 0.14
Gria3	1.06 ± 0.44	1.01 ± 0.18	0.86 ± 0.31	1.11 ± 0.14
Grin2a	1.08 ± 0.52	1.05 ± 0.34	1.04 ± 0.29	1.33 ± 0.21
Grin2d	1.10 ± 0.52	1.07 ± 0.44	1.60 ± 0.97	1.91 ± 0.71*

Table 2. (continued)

	0 ppm $AlCl_3$ (Control)		1800 ppm $AlCl_3$	
	Relative Transcript Level Normalized to		Relative Transcript Level Normalized to	
	Gapdh	*Hprt*	*Gapdh*	*Hprt*
Apoptosis				
Bax	1.02 ± 0.25	1.00 ± 0.08	0.72 ± 0.15*	0.93 ± 0.08
Bcl2	1.05 ± 0.31	1.04 ± 0.29	0.82 ± 0.45	0.99 ± 0.35
Casp2	1.02 ± 0.25	1.01 ± 0.19	1.12 ± 0.48	1.41 ± 0.35*
Casp3	1.02 ± 0.24	1.01 ± 0.17	0.89 ± 0.36	1.11 ± 0.22
Casp9	1.04 ± 0.37	1.01 ± 0.16	1.02 ± 0.45	1.27 ± 0.27
Casp12	1.09 ± 0.52	1.03 ± 0.27	0.94 ± 0.36	1.22 ± 0.38

Abbreviations: *Arc*, activity-regulated cytoskeletal-associated protein; *Bax*, BCL2-associated X protein; *Bcl2*, B-cell leukemia/lymphoma 2; *Bdnf*, brain derived neurotrophic factor; *Casp2*, caspase 2; *Casp3*, caspase 3; *Casp9*, caspase 9; *Casp12*, caspase 12; *Chrna4*, cholinergic receptor nicotinic alpha polypeptide 4; *Chrna7*, cholinergic receptor nicotinic alpha polypeptide 7; *Chrnb2*, cholinergic receptor nicotinic beta polypeptide 2; *Fos*, FBJ osteosarcoma oncogene; *Gapdh*, glyceraldehyde-3-phosphate dehydrogenase; *Gria1*, glutamate receptor, ionotropic, AMPA1 (alpha 1); *Gria2*, glutamate receptor, ionotropic, AMPA2 (alpha 2); *Gria3*, glutamate receptor, ionotropic, AMPA3 (alpha 3); *Grin2a*, glutamate receptor, ionotropic, NMDA2A (epsilon 1); *Grin2d*, glutamate receptor, ionotropic, NMDA2D (epsilon 4); *Hprt*, hypoxanthine guanine phosphoribosyl transferase; *Kitl*, kit ligand; *Notch1*, notch 1; *Ntrk2*, neurotrophic tyrosine kinase, receptor, type 2; *Pcna*, proliferating cell nuclear antigen; *Ptgs2*, prostaglandin-endoperoxide synthase 2; *Slc17a6*, solute carrier family 17 (sodium-dependent inorganic phosphate cotransporter), member 6; *Slc17a7*, solute carrier family 17 (sodium-dependent inorganic phosphate cotransporter), member 7.

Data are expressed as the mean ± SD.

*$p < .05$,

**$p < .01$, compared with the 0-ppm controls by Student's *t*-test or Aspin-Welch's *t*-test.

suggestive of the increase of synaptic plasticity of GCL. In contrast, we also found transcript downregulation of *Slc17a6* on PND 21 at 1800 ppm. On PND 77, *Slc17a6* was upregulated in this group. The highest density of boutons expressing VGLUT2, a gene product of *Slc17a6*, of mossy cells makes an axonal projection to granule cells in the dentate gyrus (Halasy *et al.*, 2004). Additionally, the highest levels of VGLUT2 are expressed in the hippocampus during the early postnatal stage to mediate glutamate release to support synaptogenesis that is necessary for hippocampal development (Boulland *et al.*, 2004). These results suggest unbalanced synaptic plasticity changes within the dentate gyrus through the adult stage.

In conclusion, developmental exposure to $AlCl_3$ via maternal drinking water decreased the NSCs in offspring, suggestive of a reflection of NSC pool exhaustion by loss of $p21^{Cip1/Waf1}$-mediated compromised cell quiescence to cause an impaired self-renewal capacity of NSCs accompanying slowing down of cell cycling. Decrease in $Reelin^+$ hilar GABAergic interneurons may also contribute to the NSC reduction. In contrast, increase of progenitor and immature granule cells suggested facilitation of transient progenitor cell proliferation and differentiation by enhancing the $PVALB^+$ interneuron signal and COX-2-mediated signals during exposure. In addition, increase of apoptosis or Morin-stained cells in the GCL, together with *Casp12* transcript upregulation, suggested an induction of Al accumulation-related ER stress-mediated granule cell apoptosis. Transcript expression changes on cholinergic and glutamatergic signals and synaptic plasticity suggested contribution to disruptive neurogenesis. The NSC-targeting effects were sustained through the adult stage despite no sustained Al-accumulation. These results suggest that developmental $AlCl_3$-exposure irreversibly affects postnatal hippocampal neurogenesis involving multiple functions in mice.

SUPPLEMENTARY DATA

Supplementary data are available at *Toxicological Sciences* online.

ACKNOWLEDGMENT

The authors thank Shigeko Suzuki for her technical assistance in preparing the histological specimens. All authors declare that there are no conflicts of interest that influenced the outcome of the present study.

FUNDING

Grant-in-Aid for Scientific Research (B) from the Japan Society for the Promotion of Science (JSPS; grant no. 25292170); Research Fund from Institute of Global Innovation Research, Tokyo University of Agriculture and Technology.

REFERENCES

Abdel Moneim, A. E. (2012). Evaluating the potential role of pomegranate peel in aluminum-induced oxidative stress and histopathological alterations in brain of female rats. *Biol. Trace Elem. Res.* **150**, 328–336.

Abu-Taweel, G. M., Jamaan, S. A., and Hossam, E. (2011). Aluminum-induced testosterone decrease results in physiological and behavioral changes in male mice. *Afr. J. Biotech.* **10**, 201–208.

Akane, H., Shiraki, A., Imatanaka, N., Akahori, Y., Itahashi, M., Ohishi, T., Mitsumori, K., and Shibutani, M. (2013). Glycidol induces axonopathy by adult-stage exposure and aberration of hippocampal neurogenesis affecting late-stage differentiation by developmental exposure in rats. *Toxicol. Sci.* **134**, 140–154.

Alaghband, Y., O'Dell, S. J., Azarnia, S., Khalaj, A. J., Guzowski, J. F., and Marshall, J. F. (2014). Retrieval-induced NMDA receptor-dependent Arc expression in two models of cocaine-cue memory. *Neurobiol. Learn. Mem.* **116**, 79–89.

Amaral, D. G., and Kurz, J. (1985). An analysis of the origins of the cholinergic and noncholinergic septal projections to the hippocampal formation of the rat. *J. Comp. Neurol.* **240**, 37–59.

Baydar, T., Papp, A., Aydin, A., Nagymajtenyi, L., Schulz, H., Isimer, A., and Sahin, G. (2003). Accumulation of aluminum in rat brain: Does it lead to behavioral and electrophysiological changes? *Biol. Trace Elem. Res.* **92**, 231–244.

Bishop, N. J., Morley, R., Day, J. P., and Lucas, A. (1997). Aluminum neurotoxicity in preterm infants receiving intravenous-feeding solutions. *N. Engl. J. Med.* **336**, 1557–1561.

Bliss, T. V., and Collingridge, G. L. (1993). A synaptic model of memory: Long-term potentiation in the hippocampus. *Nature* **361**, 31–39.

Boulland, J. L., Qureshi, T., Seal, R. P., Rafiki, A., Gundersen, V., Bergersen, L. H., Fremeau, R. T., Jr., Edwards, R. H., Storm-Mathisen, J., and Chaudhry, F. A. (2004). Expression of the vesicular glutamate transporters during development indicates the widespread corelease of multiple neurotransmitters. *J. Comp. Neurol.* **480**, 264–280.

Burrell, S. A., and Exley, C. (2010). There is (still) too much aluminium in infant formulas. *BMC Pediatr.* **10**, 63.

Chen, C., Magee, J. C., and Bazan, N. G. (2002). Cyclooxygenase-2 regulates prostaglandin E2 signaling in hippocampal long-term synaptic plasticity. *J. Neurophysiol.* **87**, 2851–2857.

Chowdhury, S., Shepherd, J. D., Okuno, H., Lyford, G., Petralia, R. S., Plath, N., Kuhl, D., Huganir, R. L., and Worley, P. F. (2006). Arc interacts with the endocytic machinery to regulate AMPA receptor trafficking. *Neuron* **52**, 445–459.

Crapper, D. R., Krishnan, S. S., and Dalton, A. J. (1973). Brain aluminum distribution in Alzheimer's disease and experimental neurofibrillary degeneration. *Science* **180**, 511–513.

De Boni, U., Scott, J. W., and Crapper, D. R. (1974). Intracellular aluminum binding; a histochemical study. *Histochemistry* **40**, 31–37.

DeVoto, E., and Yokel, R. A. (1994). The biological speciation and toxicokinetics of aluminum. *Environ. Health Perspect.* **102**, 940–951.

[EFSA] European Food Safety Authority. (2008). Safety of aluminium from dietary intake – scientific opinion of the panel on food additives, flavourings, processing aids and food contact materials (AFC). *EFSA J.* **754**, 1–34.

Eng, L. F., Ghirnikar, R. S., and Lee, Y. L. (2000). Glial fibrillary acidic protein: GFAP-thirty-one years (1969-2000). *Neurochem. Res.* **25**, 1439–1451.

Fang, F., Zhang, H., Zhang, Y., Xu, H., Huang, Q., Adilijiang, A., Wang, J., Zhang, Z., Zhang, D., Tan, Q., *et al.* (2013). Antipsychotics promote the differentiation of oligodendrocyte progenitor cells by regulating oligodendrocyte lineage transcription factors 1 and 2. *Life Sci.* **93**, 429–434.

Fleischmann, A., Hvalby, O., Jensen, V., Strekalova, T., Zacher, C., Layer, L. E., Kvello, A., Reschke, M., Spanagel, R., Sprengel, R., *et al.* (2003). Impaired long-term memory and NR2A-type NMDA receptor-dependent synaptic plasticity in mice lacking c-Fos in the CNS. *J. Neurosci.* **8**, 9116–9122.

Fonnum, F., Karlsen, R. L., Malthe-Sørenssen, D., Skrede, K. K., and Walaas, I. (1979). Localization of neurotransmitters, particularly glutamate, in hippocampus, septum, nucleus accumbens and superior colliculus. *Prog. Brain Res.* **51**, 167–191.

Freund, T. F., and Buzsáki, G. (1996). Interneurons of the hippocampus. *Hippocampus* **6**, 347–470.

Fujise, N., Liu, Y., Hori, N., and Kosaka, T. (1998). Distribution of calretinin immunoreactivity in the mouse dentate gyrus: II. Mossy cells, with special reference to their dorsoventral difference in calretinin immunoreactivity. *Neuroscience* **82**, 181–200.

Gong, C., Wang, T. W., Huang, H. S., and Parent, J. M. (2007). Reelin regulates neuronal progenitor migration in intact and epileptic hippocampus. *J. Neurosci.* **27**, 1803–1811.

Gross, A., Jockel, J., Wei, M. C., and Korsmeyer, S. J. (1998). Enforced dimerization of BAX results in its translocation, mitochondrial dysfunction and apoptosis. *EMBO J.* **17**, 3878–3885.

Guzowski, J. F. (2002). Insights into immediate-early gene function in hippocampal memory consolidation using antisense oligonucleotide and fluorescent imaging approaches. *Hippocampus* **12**, 86–104.

Halasy, K., Hajszan, T., Kovács, E. G., Lam, T. T., and Leranth, C. (2004). Distribution and origin of vesicular glutamate transporter 2-immunoreactive fibers in the rat hippocampus. *Hippocampus* **14**, 908–918.

Harrist, A., Beech, R. D., King, S. L., Zanardi, A., Cleary, M. A., Caldarone, B. J., Eisch, A., Zoli, M., and Picciotto, M. R. (2004). Alteration of hippocampal cell proliferation in mice lacking the $\beta 2$ subunit of the neuronal nicotinic acetylcholine receptor. *Synapse* **54**, 200–206.

Hodge, R. D., Kowalczyk, T. D., Wolf, S. A., Encinas, J. M., Rippey, C., Enikolopov, G., Kempermann, G., and Hevner, R. F. (2008). Intermediate progenitors in adult hippocampal neurogenesis: Tbr2 expression and coordinate regulation of neuronal output. *J. Neurosci.* **28**, 3707–3717.

Itahashi, M., Abe, H., Tanaka, T., Mizukami, S., Kimura, M., Yoshida, T., and Shibutani, M. (2015). Maternal exposure to hexachlorophene targets intermediate-stage progenitor cells of the hippocampal neurogenesis in rat offspring via dysfunction of cholinergic inputs by myelin vacuolation. *Toxicology* **328**, 123–134.

Ito, D., Imai, Y., Ohsawa, K., Nakajima, K., Fukuuchi, Y., and Kohsaka, S. (1998). Microglia-specific localisation of a novel calcium binding protein, Iba1. *Brain Res. Mol. Brain Res.* **57**, 1–9.

Kempermann, G., Jessberger, S., Steiner, B., and Kronenberg, G. (2004). Milestones of neuronal development in the adult hippocampus. *Trends Neurosci.* **27**, 447–452.

Kessels, H. W., and Malinow, R. (2009). Synaptic AMPA receptor plasticity and behavior. *Neuron* **61**, 340–350.

Khan, Z., Combadière, C., Authier, F. J., Itier, V., Lux, F., Exley, C., Mahrouf-Yorgov, M., Decrouy, X., Moretto, P., Tillement, O., *et al.* (2013). Slow CCL2-dependent translocation of biopersistent particles from muscle to brain. *BMC Med.* **11**, 99.

Kinney, J. W., Davis, C. N., Tabarean, I., Conti, B., Bartfai, T., and Behrens, M. M. (2006). A specific role for NR2A-containing NMDA receptors in the maintenance of parvalbumin and GAD67 immunoreactivity in cultured interneurons. *J. Neurosci.* **26**, 1604–1615.

Kippin, T. E., Martens, D. J., and van der Kooy, D. (2005). p21 loss compromises the relative quiescence of forebrain stem cell proliferation leading to exhaustion of their proliferation capacity. *Genes Dev.* **19**, 756–767.

Livak, K. J., and Schmittgen, T. D. (2001). Analysis of relative gene expression data using real-time quantitative PCR and the $2^{-\Delta\Delta}C_T$ method. *Methods* **25**, 402–408.

Lugert, S., Vogt, M., Tchorz, J. S., Müller, M., Giachino, C., and Taylor, V. (2012). Homeostatic neurogenesis in the adult hippocampus does not involve amplification of $Ascl1^{high}$ intermediate progenitors. *Nat. Commun.* **14**, 670.

Ma, Y., Matsuwaki, T., Yamanouchi, K., and Nishihara, M. (2017). Glucocorticoids suppress the protective effect of cyclooxygenase-2-related signaling on hippocampal

neurogenesis under acute immune stress. *Mol. Neurobiol.* **54**, 1953–1966.

Masiulis, I., Yun, S., and Eisch, A. J. (2011). The interesting interplay between interneurons and adult hippocampal neurogenesis. *Mol. Neurobiol.* **44**, 287–302.

Moazedi, A. A., Ehsani, V. S., and Chinipardaz, R. (2008). Effect of oral aluminum chloride administration during lactation on short and long-term memory of their offspring. *J. Biol. Sci.* **8**, 767–772.

Montaron, M. F., Koehl, M., Lemaire, V., Drapeau, E., Abrous, D. N., and Le Moal, M. (2004). Environmentally induced long-term structural changes: Cues for functional orientation and vulnerabilities. *Neurotox. Res.* **6**, 571–580.

Mustafa Rizvi, S. H., Parveen, A., Verma, A. K., Ahmad, I., Arshad, M., and Mahdi, A. A. (2014). Aluminium induced endoplasmic reticulum stress mediated cell death in SH-SY5Y neuroblastoma cell line is independent of p53. *PLoS One* **9**, e98409.

Nahm, W. K., and Noebels, J. L. (1998). Nonobligate role of early or sustained expression of immediate-early gene proteins c-Fos, c-Jun, and Zif/268 in hippocampal mossy fiber sprouting. *J. Neurosci.* **18**, 9245–9255.

Nam, S. M., Kim, J. W., Yoo, D. Y., Choi, J. H., Kim, W., Jung, H. Y., Won, M. H., Hwang, I. K., Seong, J. K., and Yoon, Y. S. (2015). Comparison of pharmacological and genetic inhibition of cyclooxygenase-2: Effects on adult neurogenesis in the hippocampal dentate gyrus. *J. Vet. Sci.* **16**, 245–251.

OECD Test Guideline 426. (2007). *OECD Guideline for Testing of Chemicals. Developmental Neurotoxicity Study*. Organisation for Economic Co-operation and Development, Paris, France; Available at https://www.oecd-ilibrary.org/environment/test-no-426-developmental-neurotoxicity-study_9789264067394-en. Accessed 6 April 2018.

Ozawa, S., Kamiya, H., and Tsuzuki, K. (1998). Glutamate receptors in the mammalian central nervous system. *Prog. Neurobiol.* **54**, 581–618.

Pawluski, J. L., Brummelte, S., Barha, C. K., Crozier, T. M., and Galea, L. A. (2009). Effects of steroid hormones on neurogenesis in the hippocampus of the adult female rodent during the estrous cycle, pregnancy, lactation and aging. *Front. Neuroendocrinol.* **30**, 343–357.

Priest, N. D. (1993). The bioavailability and metabolism of aluminium compounds in man. *Proc. Nutr. Soc.* **52**, 231–240.

Qiu, J., Takagi, Y., Harada, J., Rodrigues, N., Moskowitz, M. A., Scadden, D. T., and Cheng, T. (2004). Regenerative response in ischemic brain restricted by $p21^{cip1/waf1}$. *J. Exp. Med.* **199**, 937–945.

Roque, T., Haton, C., Etienne, O., Chicheportiche, A., Rousseau, L., Martin, L., Mouthon, M. A., and Boussin, F. D. (2012). Lack of a *p21waf1/cip*-dependent G1/S checkpoint in neural stem and progenitor cells after DNA damage in vivo. *Stem Cells* **30**, 537–547.

Shaw, C. A., and Petrik, M. S. (2009). Aluminum hydroxide injections lead to motor deficits and motor neuron degeneration. *J. Inorg. Biochem.* **103**, 1555–1562.

Shibutani, M. (2015). Hippocampal neurogenesis as a critical target of neurotoxicants contained in foods. *Food Safety* **3**, 1–15.

Sibbe, M., Kuner, E., Althof, D., and Frotscher, M. (2015). Stem- and progenitor cell proliferation in the dentate gyrus of the reeler mouse. *PLoS One* **10**, e0119643.

Smith, R. W. (1996). Kinetic aspects of aqueous aluminum chemistry: Environmental implications. *Coord. Chem. Rev.* **149**, 81–93.

Son, J. H., and Winzer-Serhan, U. H. (2008). Expression of neuronal nicotinic acetylcholine receptor subunit mRNAs in rat hippocampal GABAergic interneurons. *J. Comp. Neurol.* **511**, 286–299.

Struys-Ponsar, C., Kerkhofs, A., Gauthier, A., Soffié, M., and van den Bosch de Aguilar, P. (1997). Effects of aluminum exposure on behavioral parameters in the rat. *Pharmacol. Biochem. Behav.* **56**, 643–648.

Takács, S., Tatár, A., and Barkai, L. (1992). Trace elements in the human blood, cerebrospinal and amniotic fluid. *Zentralbl. Hyg. Umweltmed.* **193**, 329–341.

Tanaka, T., Abe, H., Kimura, M., Onda, N., Mizukami, S., Yoshida, T., and Shibutani, M. (2016). Developmental exposure to T-2 toxin reversibly affects postnatal hippocampal neurogenesis and reduces neural stem cells and progenitor cells in mice. *Arch. Toxicol.* **90**, 2009–2024.

Tozuka, Y., Fukuda, S., Namba, T., Seki, T., and Hisatsune, T. (2005). GABAergic excitation promotes neuronal differentiation in adult hippocampal progenitor cells. *Neuron* **47**, 803–815.

Yamasaki, M., Okada, R., Takasaki, C., Toki, S., Fukaya, M., Natsume, R., Sakimura, K., Mishina, M., Shirakawa, T., and Watanabe, M. (2014). Opposing role of NMDA receptor GluN2B and GluN2D in somatosensory development and maturation. *J. Neurosci.* **34**, 11534–11548.

Yoneda, T., Imaizumi, K., Oono, K., Yui, D., Gomi, F., Katayama, T., and Tohyama, M. (2001). Activation of caspase-12, an endoplasmic reticulum (ER) resident caspase, through tumor necrosis factor receptor-associated factor 2-dependent mechanism in response to the ER stress. *J. Biol. Chem.* **276**, 13935–13940.

Yuan, C. Y., Lee, Y. J., and Hsu, G. S. (2012). Aluminum overload increases oxidative stress in four functional brain areas of neonatal rats. *J. Biomed. Sci.* **19**, 51.

Zhao, C., Deng, W., and Gage, F. H. (2008). Mechanisms and functional implications of adult neurogenesis. *Cell* **132**, 645–660.